A THEORETICAL AND EXPERIMENTAL INVESTIGATION OF CYLINDRICAL ELECTROSTATIC PROBES AT ARBITRARY INCIDENCE IN FLOWING PLASMA

by Renaldo V. Jenkins and W. Linwood Jones, Jr.

Langley Research Center
Hampton, Va. 23665

1. Report No. NASA TR R-425	2. Government Accession No.	3. Recipient's Catalog No.
4. Title and Subtitle A THEORETICAL AND EXPERIMENTAL INVESTIGATION OF CYLINDRICAL ELECTROSTATIC PROBES AT ARBITRARY INCIDENCE IN FLOWING PLASMA		5. Report Date July 1974
		6. Performing Organization Code
7. Author(s) Renaldo V. Jenkins and W. Linwood Jones, Jr.		8. Performing Organization Report No. L-9313
9. Performing Organization Name and Address NASA Langley Research Center Hampton, Va. 23665		10. Work Unit No. 501-04-03-05
		11. Contract or Grant No.
12. Sponsoring Agency Name and Address National Aeronautics and Space Administration Washington, D.C. 20546		13. Type of Report and Period Covered Technical Report
		14. Sponsoring Agency Code

15. Supplementary Notes

16. Abstract

This report presents the theory for calculating the current collected by a negatively biased cylindrical electrostatic probe at an arbitrary angle of attack in a weakly ionized flowing plasma. The theory was constructed by considering both random and directed motion simultaneous with dynamic coupling of the flow properties and of the electric field of the probe. This direct approach yielded a theory that is more general than static plasma theories modified to account for flow.

Theoretical calculations are compared with experimental electrostatic probe data obtained in the free stream of an arc-heated hypersonic wind tunnel. The theoretical calculations are based on flow conditions and plasma electron densities measured by an independent microwave interferometer technique. In addition, the theory is compared with laboratory and satellite data previously published by other investigators. In each case the comparison gives good agreement.

17. Key Words (Suggested by Author(s)) Electrostatic probes Flowing plasma Orientation angle	18. Distribution Statement Unclassified – Unlimited STAR Category 25		
19. Security Classif. (of this report) Unclassified	20. Security Classif. (of this page) Unclassified	21. No. of Pages 40	22. Price* $3.25

A THEORETICAL AND EXPERIMENTAL INVESTIGATION OF

CYLINDRICAL ELECTROSTATIC PROBES AT ARBITRARY INCIDENCE

IN FLOWING PLASMA

By Renaldo V. Jenkins and W. Linwood Jones, Jr.
Langley Research Center

SUMMARY

This report presents the theory for calculating the current collected by a negatively biased cylindrical electrostatic probe at an arbitrary angle of attack in a weakly ionized flowing plasma. The theory was constructed by considering both random and directed motion simultaneous with dynamic coupling of the flow properties and of the electric field of the probe. This direct approach yielded a theory that is more general than static plasma theories modified to account for flow.

Theoretical calculations are compared with experimental electrostatic probe data obtained in the free stream of an arc-heated hypersonic wind tunnel. The theoretical calculations are based on flow conditions and plasma electron densities measured by an independent microwave interferometer technique. In addition, the theory is compared with laboratory and satellite data previously published by other investigators. In each case the comparison gives good agreement.

INTRODUCTION

Simplicity makes the electrostatic or "Langmuir" probe attractive for plasma diagnostics; however, the theoretical interpretation of its current-voltage characteristics is extremely complicated. Nevertheless this problem has been extensively analyzed and for the case of collisionless plasmas at rest has been adequately described. Unfortunately, the theory for interpreting the response of an electrostatic probe in a plasma with directed flow is considerably more complicated than the static case.

For years it was argued that sufficiently long cylindrical probes alined parallel to a flowing plasma responded independent of the flow. On a general scale, the credibility of this argument was severely weakened by Bettinger and Chen's publication of L. H. Brace's Langmuir probe data from the Explorer 17 satellite. (See ref. 1.) During this experiment, a probe with a length-diameter ratio of 410 exhibited an unexpected increase

in current as the axis of the probe was brought into alinement with the satellite's velocity vector. (See fig. 1.) Since this result could not be explained by any static plasma

Current, μA

$$r_p = 0.028 \text{ cm}$$
$$n_O = 5.74 \times 10^5 \text{ cm}^{-3}$$
$$n_H = 0.65 \times 10^5 \text{ cm}^{-3}$$
$$T_i = 750 \text{ K}$$
$$T_e = 2200 \text{ K}$$
$$U = 7.9 \times 10^5 \text{ cm sec}^{-1}$$
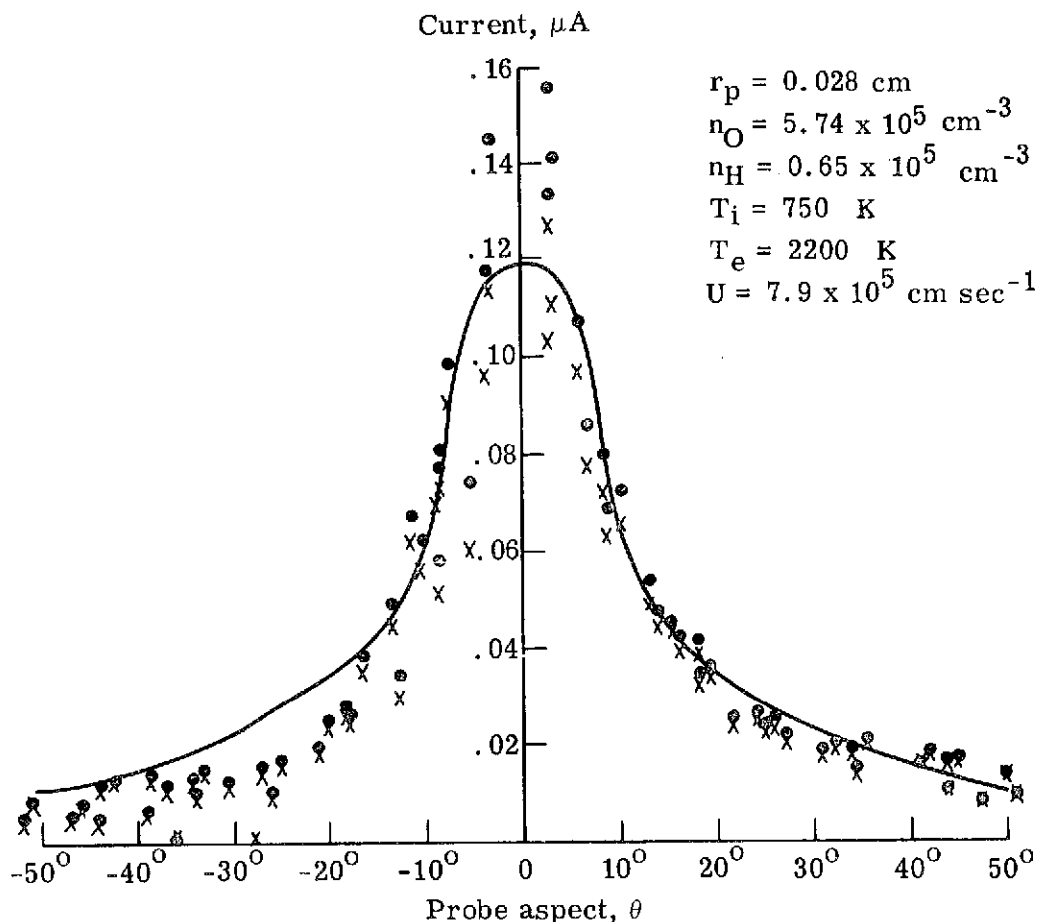
Probe aspect, θ

Figure 1.- An example of ion current peaking as published by Bettinger and Chen in reference 1 (L. H. Brace's observation). (Fit for BP 595 from ref. 1 with 10% H^+ and 90% O^+. The solid line represents the theoretical curve; the x's, the experimental curve with $\phi = K/r$; the dots, the experimental curve with $\phi = K/r^2$.)

theory, Bettinger and Chen (ref. 1) developed a new theory for flowing plasma. In their analysis the ion current peaking was explained as an end effect due to the finite length of the probe. Subsequent plasma measurements were performed by Hester and Sonin (refs. 2 and 3) under laboratory simulation of the satellite-plasma conditions. In these experiments large ion current increases, when the probe was alined with the flow (see fig. 2) were also attributed to end effects.
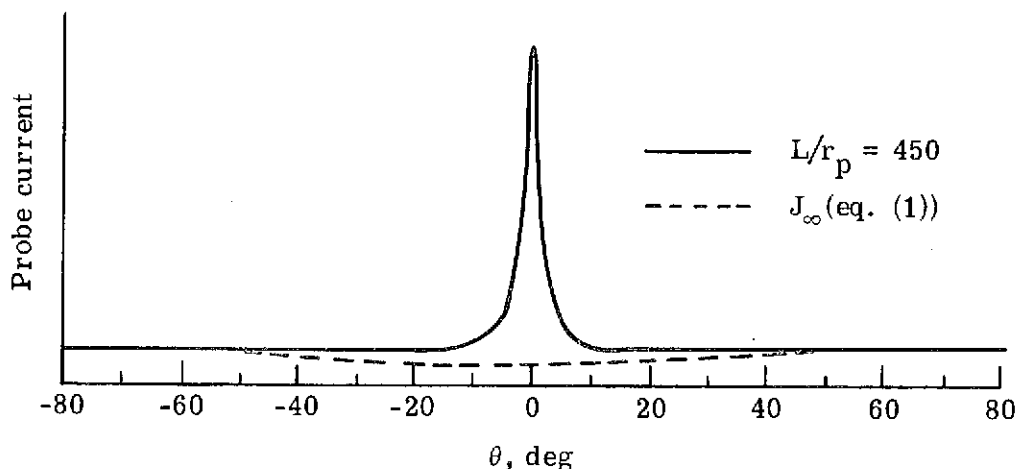
Figure 2.- End effect at a probe potential of the order of the stream energy. (Fig. 9 of ref. 3.) $U(KT_e/m_i)^{-0.5} = 38$, $\lambda_D/r_p = 13$, $e\phi_p/KT_e = -260$.

There were other flowing plasma measurements, however, which exhibited no current peaking and in which a rigorous static theory (ref. 4) modified for use in supersonic flow (refs. 5 to 7) gave convincing agreement with experimental results.

At the time when the present authors became cognizant of these references (refs. 1 to 3), they had completed both published (ref. 8) and unpublished work where probe end effects were not considered. In each case, the electron density was inferred by using both electrostatic probes and a microwave interferometer, and the agreement between the two techniques was good.

The present research was therefore undertaken to resolve whether an end effect was present for the conditions of the previous work and also to develop an improved generalized theory for calculating the positive ion current collected by a cylindrical electrostatic probe oriented at an arbitrary angle of attack in a flowing plasma.

SYMBOLS

A,B,C   empirical coefficients defined in text

d   noncollection length (see appendix A)

E   ratio of bulk flow velocity to ion velocity

$\bar{E},E_r$ electric field intensity; radial component

e   electronic charge

F	empirical factor and coefficient
G	empirical factor
I	current
J_∞	current to an infinite probe
j_e, j_i	magnitudes of electron and ion current densities at surface of a probe
K	Boltzmann's constant
L	length of probe
m	mass
N	average electron number density along microwave transmission path
n	ion or electron number density (assumed equal)
q	magnitude of electronic charge
r_p	probe radius
T	temperature
t	time
U	bulk flow velocity
V	voltage
V_+	ion velocity (approximately the speed with which ions enter the side of the Debye shield), $\sqrt{\dfrac{KT_e}{m_i}}$
ϵ_0	permittivity of free space
θ	angle of attack between probe and flow direction (called angle of orientation)

4

λ_D Debye length, $\left(\dfrac{\epsilon_o KT_e}{e^2 n}\right)^{1/2}$

ξ angle of noncollection (see appendix B)

ϕ_p difference of potential between probe and plasma

χ_p dimensionless potential difference between probe and plasma, $e(V - V_p)/KT_e$

ψ angle of collection (see appendix B)

Subscripts:

e,-   electron

end   total current contribution at zero orientation angle

i,+   positive ion

m   maximum

min   minimum

p   plasma

r   retarded

1,2   transition points

3   point at which maximum angle of collection has its minimum value

THEORY

Other Theories

A detailed review of theory and application of Langmuir probes can be found in the references by Loeb and de Leeuw (refs. 9 and 10). The original analytical expression for the ion current collected by an electrostatic probe oriented at an angle θ to plasma flow is the one by Mott-Smith and Langmuir (ref. 11). Reference 3 gives that expression as

$$J_\infty = 2enUr_pL\left(\sin^2\theta - \frac{2e\phi_p}{m_iU^2}\right)^{1/2} \qquad (1)$$

This expression, however, is only valid if the ion thermal energy is much less than the flow-directed kinetic energy $\left(KT_i \ll (1/2)m_iU^2\right)$. In the case of parallel alinement $(\theta = 0)$, the expression reduces to

$$J_\infty = 2enr_pL\left(\frac{-2e\phi_p}{m_i}\right)^{1/2} \qquad (2)$$

It so happens that this equation is also the expression for the ion current collected by a probe in a static plasma in the orbital motion limit $\left(e\phi_p \gg KT_i \gg \frac{1}{2}m_iU^2\right)$. For these conditions an infinite cylindrical probe alined parallel to flowing plasma collects ions as if the plasma were stationary.

Although this expression is inappropriate for the general case of ion collection by a probe parallel to a flowing plasma, it led to the application of other static theories to flowing plasmas. One of the most significant and realistic of these static theories is the one by Laframboise (ref. 4). This theory was developed for a two-component (ions and electrons) plasma, where each component had a Maxwellian velocity distribution.

The theory is complex and need not be thoroughly covered here, but some salient points are worth noting. The case of negative probe potential is considered primarily, since it furnishes the most information pertinent to the present investigation.

By using the mathematical framework of Bernstein and Rabinowitz (ref. 12), Laframboise (ref. 4) derived expressions for the absolute magnitude of the ion and electron current densities at the surface of a probe. For negative potentials these expressions are for the ion current density

$$j_i = en\sqrt{\frac{KT_e}{2\pi m_i}}\ I'\left(\chi_p, \frac{r_p}{\lambda_D}, \frac{T_i}{T_e}\right) \qquad (3)$$

and for the electron current density

$$j_e = en\sqrt{\frac{KT_e}{2\pi m_e}}\ \exp(\chi_p) \qquad (4)$$

From this last expression Laframboise (ref. 4) showed that the electron temperature could be determined from a semilog plot of j_e against V; this result agreed with

6

Langmuir's original conclusion. He was able to obtain this result since for slightly negative potential

$$\left| \frac{d\left[\log_e(j_e)\right]}{dV} \right| = \left| \frac{e}{KT_e} \right| \tag{5}$$

The electron temperature is therefore easily obtained from this theory but the ion number density is not.

From equation (3)

$$n = \frac{j_i}{e \sqrt{\frac{KT_e}{2\pi m_i}} \, I'\left(\chi_p, \frac{r_p}{\lambda_D}, \frac{T_i}{T_e}\right)} \tag{6}$$

The calculation of n from this equation is complicated by the fact that the dimensionless current I' is dependent on n through λ_D. Thus, n can only be computed through a tedious iterative procedure. Fortunately, Sonin (ref. 5) developed an algorithm for calculating n which was much more satisfactory than the iterative procedure.

Sonin's algorithm was evaluated experimentally in supersonic flow (refs. 5 to 7) and gave convincing results. The publication of Brace's observation by Bettinger and Chen (ref. 1), however, invalidated its applicability in certain flowing plasmas. Subsequently, Hester and Sonin (ref. 5) also confirmed Brace's results in a wind tunnel.

In references 1 and 3, theoretical analyses are included which explain the observed peaking of the ion current. Although they each attributed the peaking to end effect, they disagree on certain points. Furthermore, neither theory is generally applicable to flowing plasma. Therefore, the present theory was developed to be applicable in a more general sense to flowing plasma.

Present Theory

A theory applicable to flowing plasma must account for flow dynamics. In the present theory flow dynamics have been included by the consideration of such things as flow velocity, probe angle of attack, flow-directed kinetic energy, side collection, angle of collection, and so forth. The inclusion of such dynamic considerations has resulted in a theory widely applicable to flowing plasma.

This report restricts the theory presented to the negative potential difference $\left(\phi_p < 0\right)$ region of the probe response curve. (See fig. 3.) Although this theory should
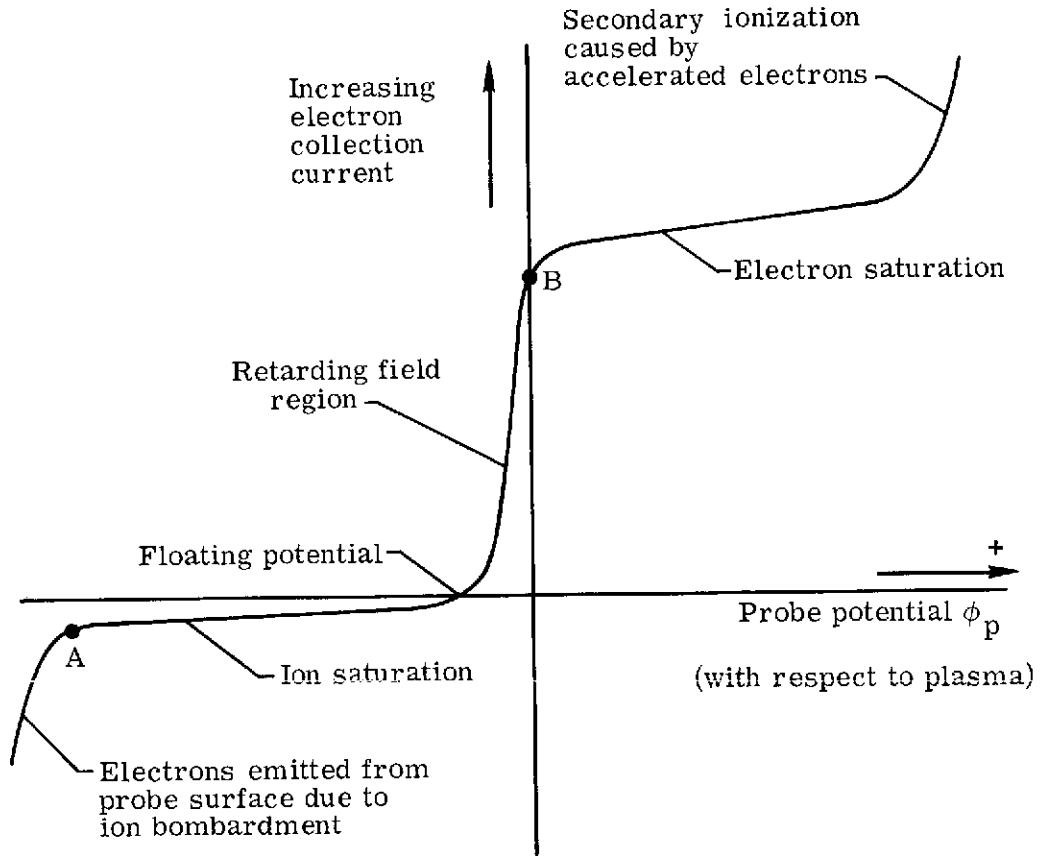
Figure 3.- Complete Langmuir probe characteristic. Ion current exaggerated.
Theory of present report restricted to region between points A and B.

be extendable to the region of positive ϕ_p, such an extension is beyond the scope of this work.

The theory is relegated to two distinct classes. The names and criteria for these classes are as follows:

Class I – Thermal: With probe at an angle of attack of 0°, the probe current must be dominated by particles that enter the Debye shield as a result of random thermal motion. Thus, the particle flow-directed kinetic energy $\frac{1}{2} m_i U^2$ is much less than the thermal energy KT_i.

Class II – Flow directed: With probe at an angle of attack of 0°, the probe current must be dominated by particles that enter the Debye shield as a result of flow-directed motion. Here the kinetic energy $\frac{1}{2} m_i U^2$ is much greater than the thermal energy KT_i.

Notice that the criteria do not exclude particle contribution by thermal or flow-directed motion from either class. This nonexclusion is mandated by the physical reality that no flowing plasma is without both types of motion.

The theory was developed by use of the following steps:

(1) Assume that the Debye shielding length concept is valid for any charged body whose characteristic dimension (probe diameter here) is less than the mean free path of the plasma. Thus, only the charged particles within the Debye shield can be affected by the probe.

(2) List the ways in which ions on electrons could enter the Debye shield, that is, ions enter the shield's end as a result of flow-directed motion.

(3) Construct current contribution terms by using the list of step 2, that is, the end ion current is $enU(r_p + \lambda_D)^2\pi \cos \theta$. (The ideal current is the algebraic sum of all such terms.)

(4) Determine whether any of the terms of the ideal current should be eliminated for physical reasons. (Example: The flow-directed electrons entering the end of the shield have insufficient kinetic energy to overcome the electric field, except for very small potential differences. Under this condition there is a physical basis for eliminating the end electron current contribution terms.)

(5) Modify the current contribution terms where necessary to account for such items as maximum angle of collection, true collection length, and the effect of the various velocities on particle collection.

In some instances the modifications of step (5) took the form of semiempirical coefficients and factors. The term semiempirical is used since these coefficients and factors are computed from physical properties of the plasma or are the decade normalization of such computations.

Thermal (Class I)

The derived expression for calculating the current collected by a negatively biased probe at small angles of attack $(0^O < \theta < 15^O)$ is

$$
\begin{aligned}
I = {} & 2en\pi\left(r_p + \lambda_D\right)\left(L - d_+ \cos \theta\right)\left(V_+\right) \\
& - 2en\pi\left(r_p + \lambda_D\right)\left(L - d_{-r} \cos \theta\right)\left(V_-\right)\exp\left(-e\phi_p/KT_e\right) \\
& + enU\left(r_p + \lambda_D\right)^2\pi \cos \theta - enU\left(r_p\right)^2\pi \cos \theta \\
& + 2enL\left(r_p + \lambda_D\right)\left(\sin \psi_m\right)^E\left(V_+\right)\theta^F - 2enL\left(r_p\right)U \sin \theta
\end{aligned}
\tag{7}
$$

The first and second terms represent the currents due to ions and electrons, respectively, that enter the Debye shield as a result of thermal motion. The effect of

flow dynamics is included through the quantities d_+ and d_{-r} (ion and electron non-collection lengths). These factors must be included because in the time required for the charged particles to reach the probe surface, the ions and electrons move downstream these lengths. (Expressions for computing d_+ and d_{-r} are derived in appendix A.) The third and fourth terms are end currents due, respectively, to flow-directed ions and electrons.

The fifth and sixth terms are the flow-directed currents collected by the probe side area. The variables ψ_m and θ of the fifth term are introduced to account for the modified capture area and efficiency of the probe while at an angle of attack. (See appendix B.) The exponent E is used to weight the angle-of-attack effect and is defined as the ratio of the bulk flow velocity to the ion velocity, $E = \dfrac{U}{V_+}$.

It was empirically determined that the coefficient F is related to E by the equation $F = \dfrac{E}{p(10)}$, where p is the decade in which E occurs. Mathematically, F can be regarded as simply the normalization of E, where the normalizing factor is the largest E of the decade which contains E. $\Big($Examples: if $E = 4.6$, then $F = \dfrac{E}{10} = \dfrac{4.6}{10} = 0.46$; if $E = 13.7$, then $F = \dfrac{13.7}{2(10)} = 0.685.\Big)$

The fourth and sixth terms are not present if $\left|\dfrac{1}{2} m_e (U \cos \theta)^2\right|$ and $\left|\dfrac{1}{2} m_e (U \sin \theta)^2\right|$ are each less than $|e\phi_p|$. Usually this is the case; therefore, they can be neglected. For large $\phi_p < 0$, the second term can also be neglected.

At zero angle of attack almost all the probe current is contributed by the first and second terms since Class I − Thermal is being considered. Note that the side collection (fifth) term dominates the shaping of the ion current as a function of orientation angle θ.

Flow-Directed Class II Theory

This class consists of two subclasses determined by the ratio E of the bulk flow to the ion velocity. For subclass A this ratio is less than 10, whereas for subclass B it is greater than 10. The theory presented for each subclass is applicable in the ion-saturation region of the response curve only. (See fig. 3.)

These subclasses came about as the result of the observation that the empirical multiplying factor, in the derived equation for ion current, must be different for the different E ratio groups. A transition E of 10 was suggested by the fact F (the decade normalization E) has a value of 1 for the first time at $E = 10$. An analytic search for further transition E ratios was fruitless; thus, it was concluded that only these two subclasses exist.

<u>Subclass A</u>.- The ion current is

$$I = GenU(r_p + \lambda_D)^2 \pi \cos \theta + 2FenL(r_p + \lambda_D)(\sin \psi_m)^A(\sin \psi_{min})^B U^F(\sin \theta)^C \quad (8)$$

Here the effects of flow are included both directly (through U the flow velocity) and indirectly (by means of the multiplying factor G). The factor G is an empirically determined end collection efficiency defined in a subsequent paragraph. It depends not only on flow properties but on probe orientation angle as well.

As a first cut, one would intuitively surmise the side collection term (term 2) to be $2enL(r_p + \lambda_D)U \cos \theta$. Note, however, that this form of the term can be true only if all the flow-directed ions entering the Debye shield from the side are collected. In reality total collection is an impossibility since some of the ions have sufficient momentum to take them outside the shield. Thus, the angle of collection and the efficiency of collection must be accounted for. This accounting is accomplished through the introduction of the efficiency coefficient F and the sine of the maximum angle of collection ψ_m. As the angle of orientation θ increases, ψ_m decreases until it reaches its minimum value of ψ_{min}. For orientation angles above the angle where this occurs, the side current becomes more directly dependent on θ, and thus $\sin \theta$ is included. The roles played by the coefficients A, B, and C in the shifting of importance of $\sin \psi_{min}$, $\sin \theta$, and $\sin \psi_m$ will become clear later when they are defined.

The factor G equals $F = \dfrac{E}{10}$ for angles of attack between 0° and the angle (in degrees) numerically equal to approximately $(E/2) + 1$. From this angle to the first transition point angle θ_1, G equals zero. Higher angles of attack $(\theta > \theta_1)$ have G equal to $1 - F$. The first transition point angle is the angle θ_1 at which the exponential coefficients A, B, and C make their first value change.

The values of A, B, and C are defined as follows:

$$\left.\begin{matrix} A = E \\ B = 0 \\ C = 0 \end{matrix}\right\} \qquad \left(\sin \psi_m > \exp\left(\frac{\log_e \sin \psi_{min}}{E - 1}\right)\right)$$

The coefficients A, B, and C initially have these values when $\theta = 0$.

$$\left.\begin{matrix} A = 1 \\ B = 1 \\ C = 0 \end{matrix}\right\} \qquad \left(\sin \psi_m < \exp\left(\frac{\log_e \sin \psi_{min}}{E - 1}\right)\right)$$

The equations for ψ_m and ψ_{min} are presented in appendix B.

$$
\left.\begin{array}{l} A = 0 \\ B = 1 \\ C = 1 \end{array}\right\} \qquad \left(\sin \psi_m < \exp\left(\frac{\log_e \sin \psi_{min}}{E - 1}\right) \text{ and } \sin \theta_2 = \sin \psi_m\right)
$$

Thus it can be seen that there are two possible transition points (from definition (1) to (2) and from (2) to (3)). One occurs at

$$
\sin \psi_m = \exp\left(\frac{\log_e \sin \psi_{min}}{E - 1}\right)
$$

and the other at

$$
\sin \psi_m = \sin \theta_2
$$

(These points are called, respectively, transition points 1 and 2.) Transition point 2 may not occur since the conditions that

$$
\sin \theta_2 = \sin \psi_m
$$

and

$$
\sin \psi_m < \exp\left(\frac{\log_e \sin \psi_{min}}{E - 1}\right)
$$

must be simultaneously satisfied for it to do so. Transition 2 can only take place after transition 1, even though the requirement $\sin \psi_m = \sin \theta_2$ is met.

As is shown in appendix B, each angle of orientation θ has a maximum angle of collection ψ_m associated with it; therefore, the transition point angles can be uniquely determined.

The shaping of the curve of ion current against θ is determined by the side collection (second) term.

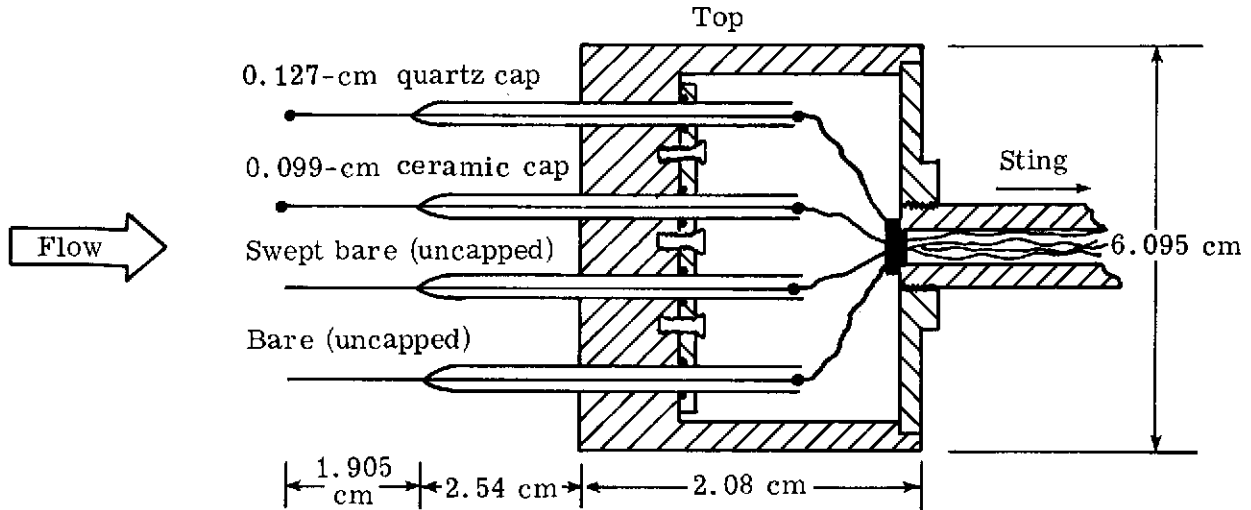Subclass B.- This subclass has an E ratio greater than 10, and the ion current is

$$
I = \left[1 + (1 - F)\right]enU(r_p + \lambda_D)^2 \pi \cos \theta
$$
$$
+ \left[1 + (1 - F)\right]2enL(r_p + \lambda_D)(\sin \psi_m)^A (\sin \psi_{min})^B (\sin \theta)^C (U)^F \tag{9}
$$

The exponential coefficients A, B, and C retain the same definitions as were given for subclass A. Here the curve shaping is also dominated by the side collection (second) term.
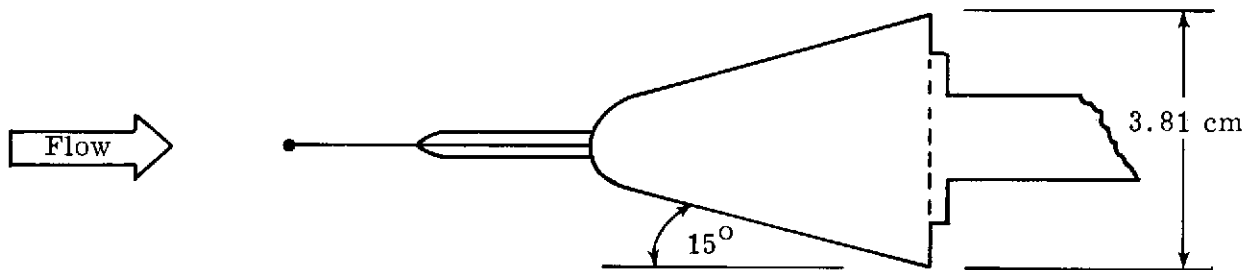
12

EXPERIMENTAL APPARATUS

Electrostatic Probe Array

The probe array used in this investigation consisted of four electrostatic probes protruding from a 15° half-angle wedge with a rounded vertex angle. Figure 4 gives two

Top

0.127-cm quartz cap

0.099-cm ceramic cap

Sting

Flow

Swept bare (uncapped)

6.095 cm

Bare (uncapped)

1.905 cm   2.54 cm   2.08 cm

(a) Cross-sectional slice of electrostatic probe array. (Side view.)

Flow

3.81 cm

15°

(b) Top view of probe array.

Figure 4.- Electrostatic probe array.

views of the array. Each probe consisted of two main parts: a 0.0254-cm-diameter tungsten electrode, and an insulator holder fashioned from 0.3-cm-diameter glass or quartz tubing. In addition, two probes of the array had a third part, an insulator cap. The top probe had a 0.127-cm-diameter quartz cap. (See fig. 4(a).) The adjacent probe had a 0.099-cm-diameter ceramic cap. The capped probes had exposed lengths identical to the 1.905-cm exposed lengths of the uncapped probes. Thus, each probe had a length-diameter ratio of 75.

The two capped probes and one of the bare probes were each fixed biased negatively with respect to the tunnel walls, and during a run an oscillograph was used to record the probe current. This recording was accomplished by using the circuitry of figure 5. The remaining uncapped probe was swept biased to record the entire voltage-current characteristic. The experimental circuit (fig. 6) utilized a linear voltage sweep from approximately -6 V to 2 V during a period of 1 to 10 milliseconds. Both the voltage
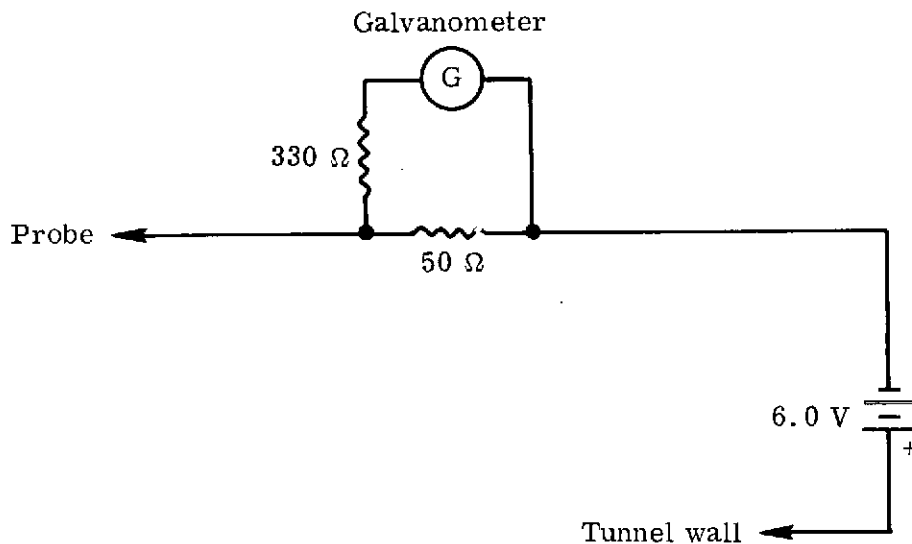
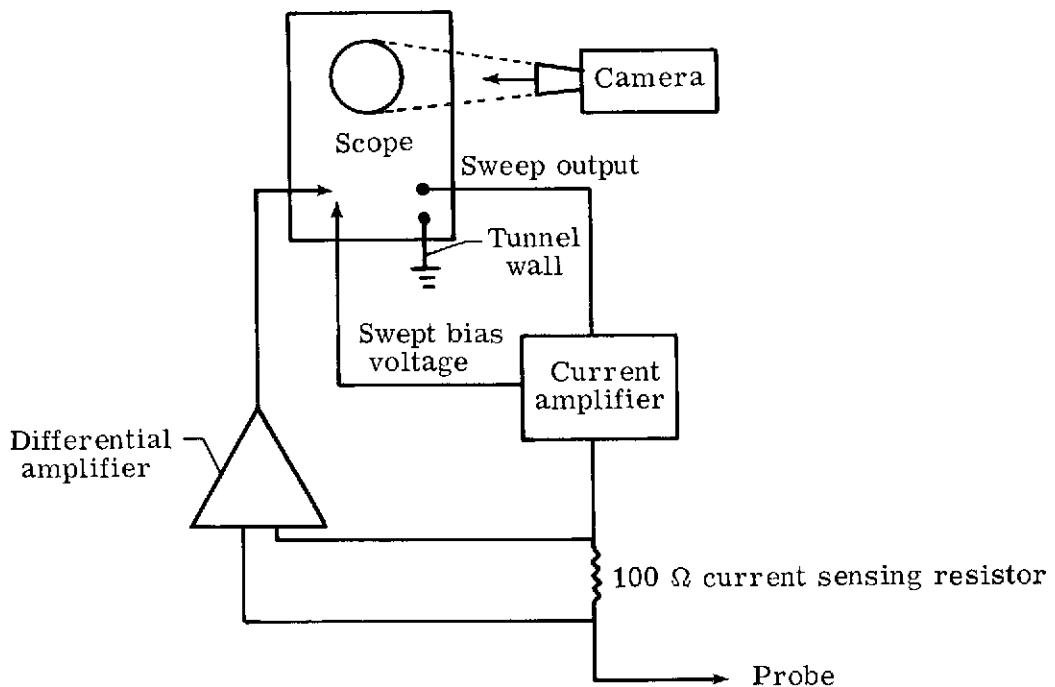Figure 5.- Circuitry for a fixed biased electrostatic probe.

Figure 6.- Block diagram of swept probe setup.

and current waveforms were displayed on a dual-beam scope where they were photographed by a high-speed framing camera.

The number of probes in the array was later reduced to two. Both of these were bare, one fixed and the other swept biased. They were located in the two center positions of the array. (See fig. 4(a).) The capped probes were removed to eliminate the cap shock waves. Visually, only the 0.127-cm-diameter quartz cap had a detectable shock; however, because of the uncertainty in shock interference, both capped probes were removed.

Microwave Interferometer

A 10-GHz microwave interferometer was used to measure independently the electron number density in the plasma flow. A discussion of microwave interferometer theory can be found in references 8, 13, and 14; but fundamentally, the interferometer is a bridge circuit which compares the phase of the data path signal with that of the reference path signal. The data path signal undergoes a negative phase shift relative to the undisturbed reference path signal as it transverses the plasma. This phase shift is related to the average electron density along the microwave transmission path by the following equation:

$$N = 7.38 \times 10^8 \, \Delta\gamma \text{ electrons/cm}^3 \tag{10}$$

where $\Delta\gamma$ is the phase difference in degrees.

A diagram of the experimental arrangement is shown in figure 7. Note in this diagram that the transmitting and receiving horn antennas are surrounded by microwave absorbing material. This material eliminated multipath propagation by absorbing microwave energy that could have otherwise been reflected off the tunnel walls. Such multipath propagation would have resulted in erroneous phase shift measurement.

As a further guard against multipath effect, the stainless-steel wedge of the probe array was positioned a minimum of 12.065 cm downstream of the microwave beam. This wedge position located the probe tips 7.62 cm downstream of the microwave path. Rotating and pivoting the probe array at this location did not affect the phase of the microwaves in the absence of plasma and thereby indicated that the probe array produced no measurable multipath effects.
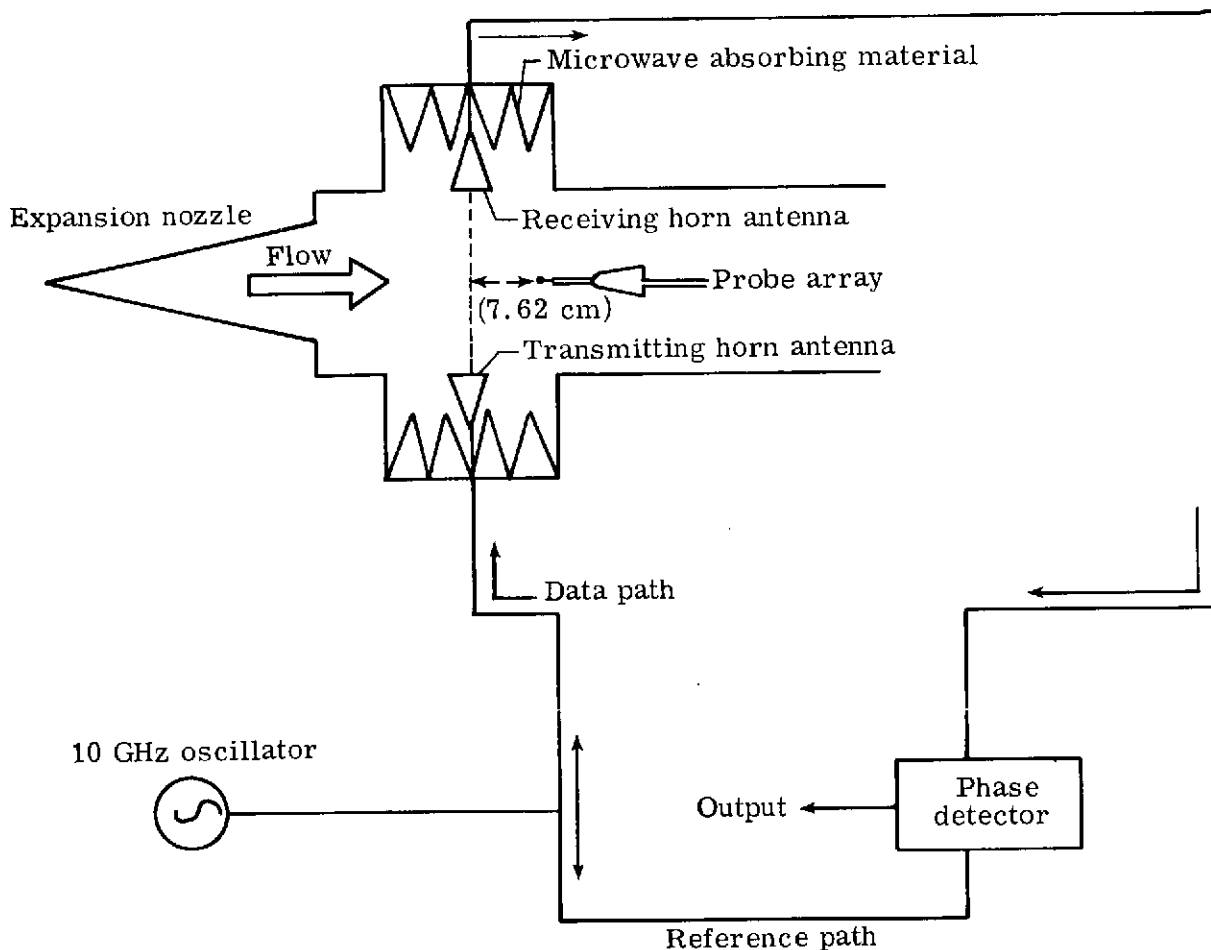
Microwave absorbing material

Expansion nozzle

Flow

Receiving horn antenna

Probe array

(7.62 cm)

Transmitting horn antenna

Data path

10 GHz oscillator

Output

Phase detector

Reference path

Figure 7.- Diagram of microwave interferometer apparatus in test section.

Description of Facility

A diagram of the Langley 1-foot hypersonic arc tunnel (30.5 cm) is shown in figure 8, and a description of the tunnel can be found in references 15 and 16. The electric arc-heated air is expanded through a conical nozzle and produces a low-density flow at a nominal Mach number of 12 in the test section. An analysis of the accuracy of the test conditions in this facility is given in reference 17.

In this test series, the facility was operated at stagnation pressures of 0.507 to 0.709 MN/m^2 with stagnation enthalpies of 6.1 to 9.8 MJ/kg. This mode of operation resulted in bulk test stream velocities of 2.98 to 3.71 km/sec.
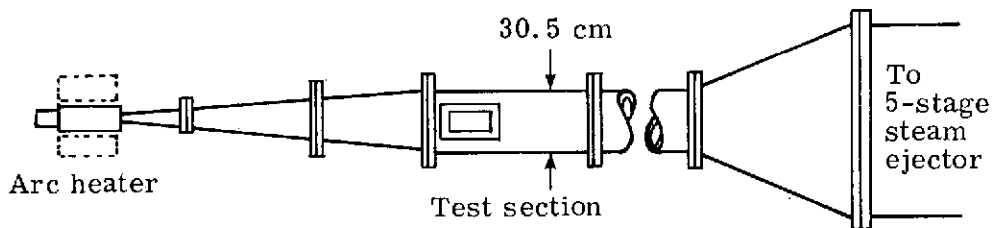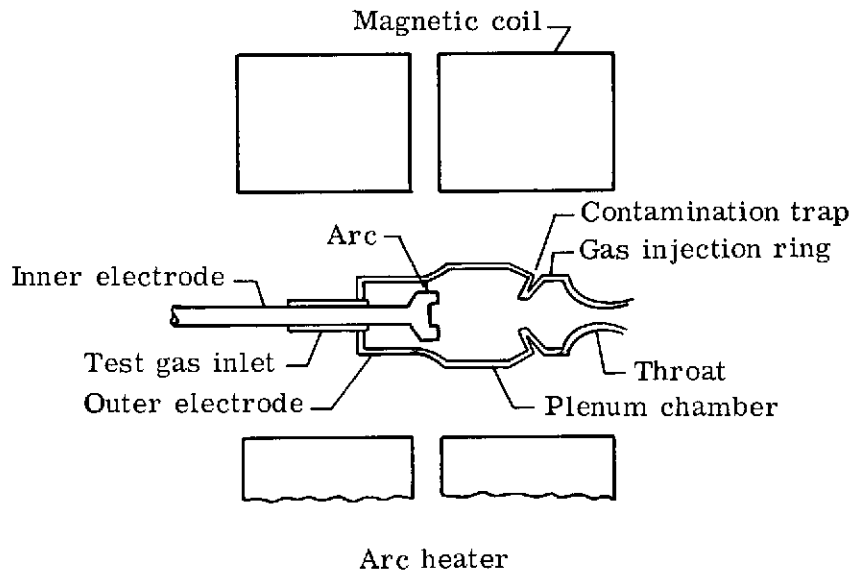
Arc heater

Figure 8.- Schematic drawing of the Langley 1-foot
hypersonic arc tunnel (30.5 cm).

RESULTS AND DISCUSSION

Experimental Search for End Effect

An interesting but inconclusive part of this work was an experimental attempt to detect probe end effects. The scheme of detection was based on the hypothesis that in the presence of end effect, probes without end current contribution should have curves of ion current against angle of attack very different in shape from those with end current. Thus, the electrostatic probe array was designed to eliminate the end ion current for certain probes. This design was accomplished by capping two probes of the array as

previously described. To be effective, these insulator caps had to prevent ions from reaching the physical end of the probe and also had to eliminate the ions that would otherwise enter the end of the Debye shield. To accomplish this, the diameter of the insulator cap should have been a minimum value of twice the sum of the probe radius and the Debye length $2(r_p + \lambda_D)$.

Insulator caps with such diameters were almost certain to produce shock waves which could invalidate the experiment. Nevertheless the end blocking criteria were used to determine the minimum cap diameter. The 0.099-cm ceramic cap had no visually detectable shock; therefore, the experiment proceeded on the assumption that if any shock was present, it was a weak conical shock. And as such, it would not appreciably change the flow angle.

During the experiment the angle of attack of the probe array was varied and the ion currents for one capless and two capped probes of the array were simultaneously recorded. Runs were conducted both with air and with nitrogen as test media. The result of one such air test is presented in figure 9. In this typical figure, the ion current for each probe is plotted against angle of attack. The diamond, square, and circular symbols, respectively, represent data for capless, 0.099-cm-diameter ceramic-capped, and 0.127-cm-diameter quartz-capped probes. The magnitudes of these currents are different; however, their shapes are strikingly similar. This result seems to be an indication of the absence of end effect. This position is further supported by the "valleying" present for each of the probe currents. Such valleying is directly opposite to the proposed end effect peaking of references 1 to 3.

A comparison of the pertinent test conditions for the present experiments and those of references 1 and 3 is given in table I. Theoretical considerations for the cylindrical

TABLE I.- PERTINENT TEST CONDITIONS

Source	n, electrons/m^3	λ_D, m	Neutral-neutral mean free path, m	r_p, m	L, m	U, m/sec
Present report	[a]3.9×10^{15} $[3.5 \times 10^{15}$ to $1.2 \times 10^{16}]$	[a]5.47×10^{-5} $[3.92 \times 10^{-5}$ to $5.83 \times 10^{-5}]$	$>5.5 \times 10^{-4}$	1.27×10^{-4}	1.905×10^{-2}	[a]3.17×10^3 $[2.98 \times 10^3$ to $3.71 \times 10^3]$
Bettinger and Chen (ref. 1)	6.39×10^{11}	4.107×10^{-3}	≈ 1236	2.8×10^{-4}	0.23	7.9×10^3
Hester and Sonin (ref. 3)	[b](1) 3.19×10^{11} [b](2) 2.69×10^{12} [b](3) 2.69×10^{13}	1.651×10^{-3}	All mean free paths were larger than the test chamber dimensions	1.27×10^{-4}	5.715×10^{-2}	[b](1) 7 753 [b](2) 21 232 [b](3) 67 143

[a]Value corresponds to data of figure 9. Bracketed values give range for present test series.

[b]These values not given, but computed by assuming ion temperatures of (1) 2 K, (2) 15 K, and (3) 150 K and $T_e = T_i \times 10^2$.

probe geometry are well satisfied (length to probe radii range from 150 to 821). The neutral-neutral mean free paths are several orders of magnitude greater for references 1 and 3 than for the present experiments. The plasma electron densities were several orders of magnitude lower in references 1 and 3 as compared with the present work. The ratios of probe radii to Debye length were less than unity for references 1 and 3 and approximately one and a half decades less than the ratio for the present experiments.
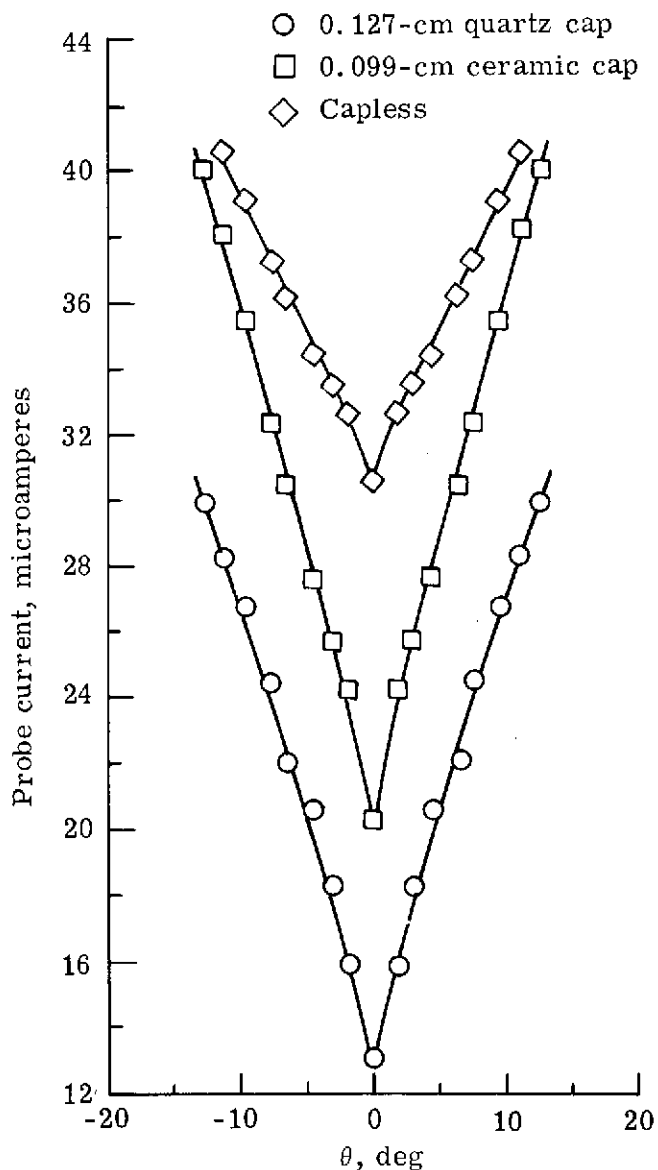

Figure 9.- Variation of ion current with angle of attack for capped and capless probes.

Measured Electron Concentration and Temperature

The microwave and electrostatic probe studies were made in the free stream of the Langley 1-foot hypersonic arc tunnel (30.5 cm). Electron number densities of 3.5×10^{15} to 1.2×10^{16} electrons/m^3 were measured by using the nonperturbing microwave interferometer. The values of electron concentration obtained by applying Laframboise's theory (ref. 4) through the use of Sonin's algorithm to parallel swept electrostatic probe data agreed within 10 percent, and suggested the validity of Laframboise's (Sonin's algorithm) theory for the flowing plasma. The semilog plotting method was used to determine the electron temperature. This method yielded electron temperatures of 2100 K to 3870 K.

Application of Present Theory

In this section the general theory of this report is applied to data representing each class. In each case, the ion current for a fixed bias probe was computed and compared with the measured ion current. The test series by the present authors furnishes the data for Class I (thermal). Class II, subclass A data are from the report by Bettinger and Chen (ref. 1), and the data for Class II, subclass B is that of Hester and Sonin (ref. 3).

Class I (thermal).- The data for one air and one nitrogen test are used. The free-stream conditions for the air test were as follows:

(1) $n = 3.68 \times 10^{15}$ electrons/m^3 (microwave interferometer)

(2) $T_e = 3020$ K (semilog plotting method)

(3) $V_+ = 915$ m/sec

(4) $U = 3.18$ km/sec

(5) The ions were NO^+.

The bulk flow velocity U was not measured, but was obtained from figure 10. This figure is a calibration plot of stagnation enthalpy against the free-stream velocity taken from the work of Guy (ref. 18) for the Langley 1-foot hypersonic arc tunnel (30.5 cm) with air as the test medium.

The ion current collected by the bare fixed bias $\left(V = -6 \text{ volts; } \phi_p = -7.5 \text{ volts}\right)$ probe for various angles of attack is shown in figure 11 as circular symbols. The solid curve of this figure is the ion current computed from theory (eq. (7)). Since the probe was negatively biased into the ion saturation region, only the first and fifth terms of the equation are significant.

As can be seen in figure 11, the theoretically predicted current is in good agreement with the measured current.
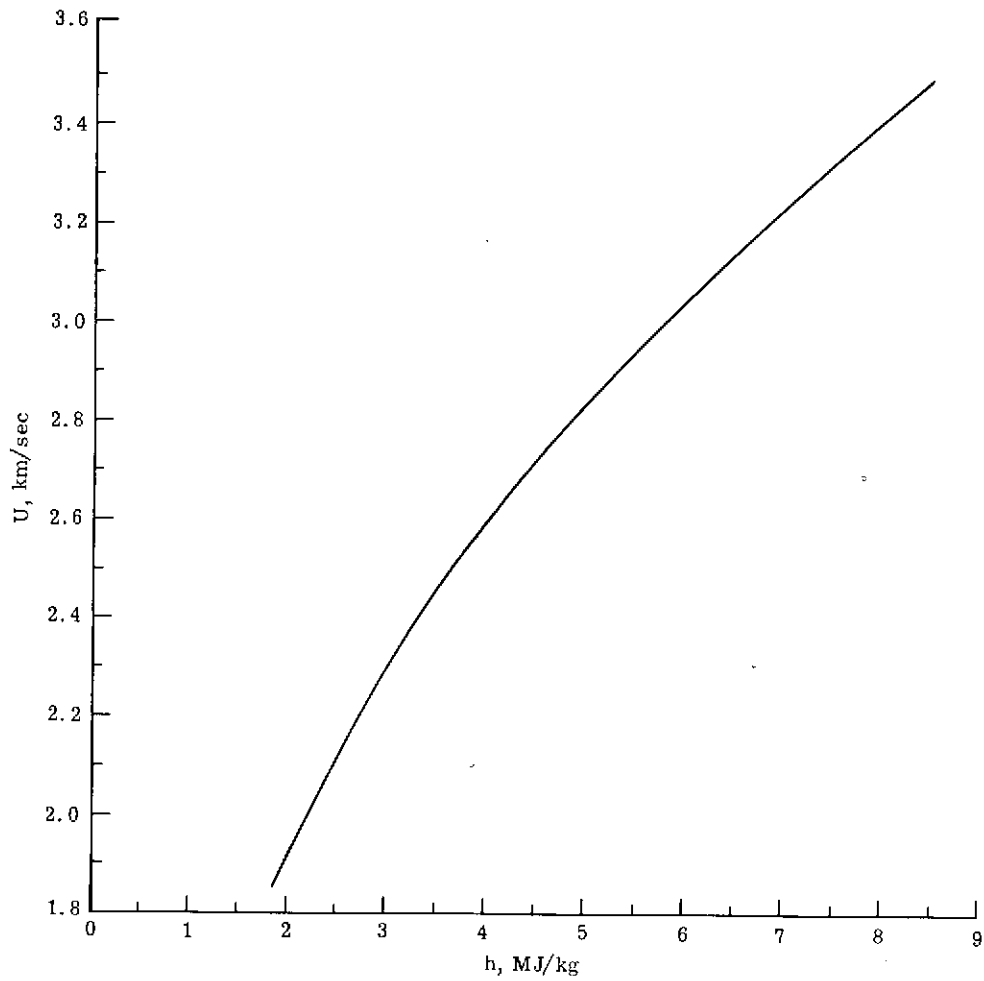
Figure 10.- A calibration plot of the variation of stagnation enthalpy with free-stream flow velocity for air test medium.
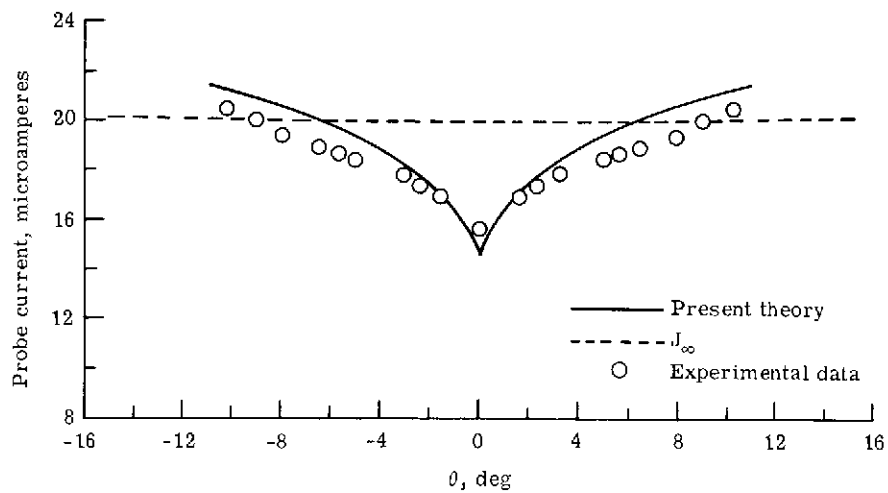

Figure 11.- Variation of ion current with angle of attack. (Test medium, air.)

Listed below are the free-stream conditions for the nitrogen run.

(1) $n = 4.36 \times 10^{15}$ electrons/m^3 (microwave interferometer)

(2) $T_e = 2761$ K (semilog plotting method)

(3) $V_+ = 1280$ m/sec

(4) $U = 3.06$ km/sec

(5) The ions were N$^+$.

The ion current measured with a fixed bias $\left(V = -6 \text{ volts;} \quad \phi_p = -7.39 \text{ volts}\right)$ bare probe is shown in figure 12. The solid curve is the calculated current. The value of bulk flow velocity U used is slightly high since it was obtained from figure 10 and is for air, and nitrogen is the test medium for the results shown in figure 12. (An unpublished nitrogen curve produced by Guy gives approximately the same velocities for air and nitrogen when the stagnation pressure is the same. Lower stagnation pressure as is the case for this nitrogen run gives slightly lower velocity.)
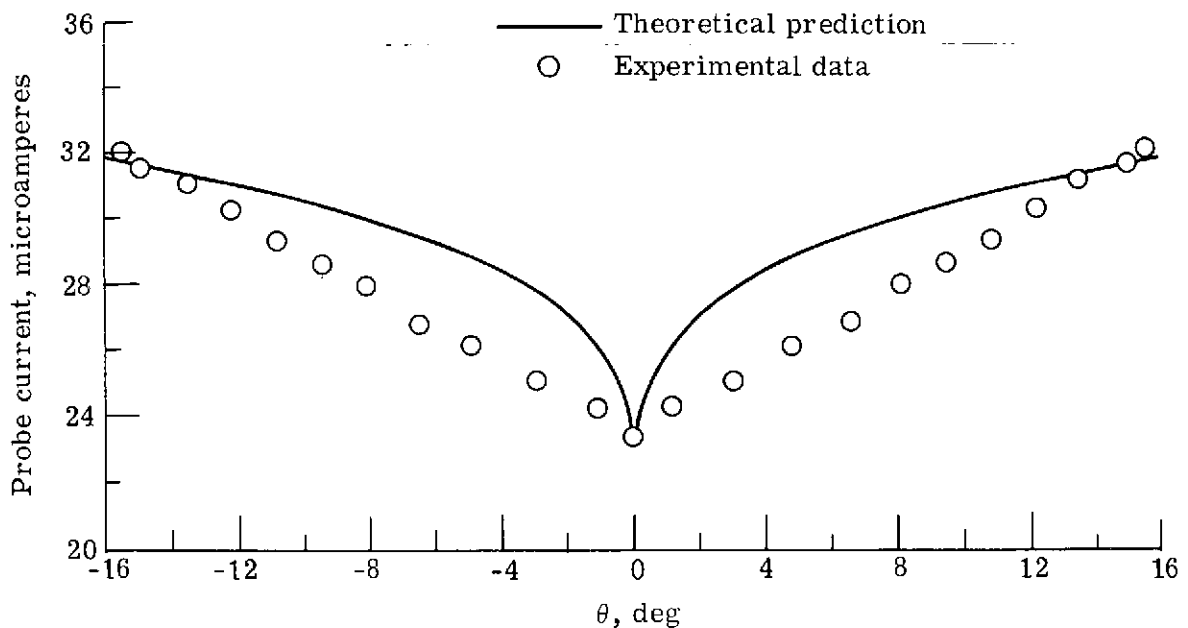

Figure 12.- Variation of ion current with angle of attack. (Test medium, nitrogen.)

The theoretical current was therefore expected to be slightly high because of the flow velocity error. Figure 12 shows the disagreement to never be greater than 10 percent. The primary point of disagreement is the shape of the two curves. From equation (7) it is apparent that the shaping of the theoretical curve is dominated by θ^F (fifth term). The quantity F equals U divided by $10V_+$, and U is thus the shaping factor. The lower (true) flow velocity would give better agreement between the shapes of

the theoretical and measured currents. (Data for tests using nitrogen with stagnation pressure compatible with fig. 10 gave curve shape agreement like that in fig. 11.)

Class II, subclass A.- The data of Bettinger and Chen (ref. 1) are presented in figure 1 (which is fig. 8 of ref. 1). In addition to the data $\left(r_p, \ T_i, \ T_e, \text{ etc.}\right)$ of this figure, the probe length L and ϕ_p are given $\left(L \text{ directly as 23 cm and } \phi_p \text{ indirectly as}\right.$ $\phi_p = 0.25 \dfrac{m_i}{e} U^2\bigg)$. Taking the ions as 0+ gives ϕ_p as -5.17 volts. Applying equations (A11) and (A12) to the data results in t_+ and d_+ values of 9.085×10^{-7} sec and 7.177 mm. The data can also be used to compute:

$$V_+ = 1069 \text{ m/sec}$$

$$E = \frac{U}{V_+} = 7.39$$

$$\lambda_D = 4.107 \text{ mm}$$

$$F = \frac{E}{10} = 0.739$$

$$\frac{E}{2} + 1 = 4.69^O$$

$$G = 0.739 \qquad\qquad (0 < \theta < 4.69^O)$$

By using equation (B3), the minimum angle of collection ψ_{min} is found to be 3.65^O. The orientation angle θ_3 at which ψ_{min} occurs is obtained from equation (B2) as 37.58^O. By solving equations (B7) and (B13), the angles of attack θ_1 and θ_2 at which transitions 1 and 2 occur are found to be, respectively, 27.67^O and 31.43^O. Since the first transition point angle θ_1 has been found, the factor G can now be specified for the complete range of θ as

$$G = \begin{cases} 0.739 & (0 < \theta \leqq 4.69^O) \\[2mm] 0 & (4.69^O < \theta \leqq 27.67^O) \\[2mm] 0.261 & (27.67^O < \theta \leqq 90^O) \end{cases}$$

With these computations completed, equation (8) can be utilized and the theoretical ion current for various angles of attack can be calculated. The current so calculated is

23

presented in figure 13. A comparison of the theoretical curve of this figure with the experimental data of figure 1 gives good agreement. The slight disagreement that does exist is for angles above 5° or below -5° and should be attributed to the fact that the experimental data have not been corrected to account for the difference in ϕ_p for these angles of attack. This difference in ϕ_p is a consequence of the slowly varying swept voltage applied to the probe; that is, the experimental data were not obtained with a fixed ϕ_p.
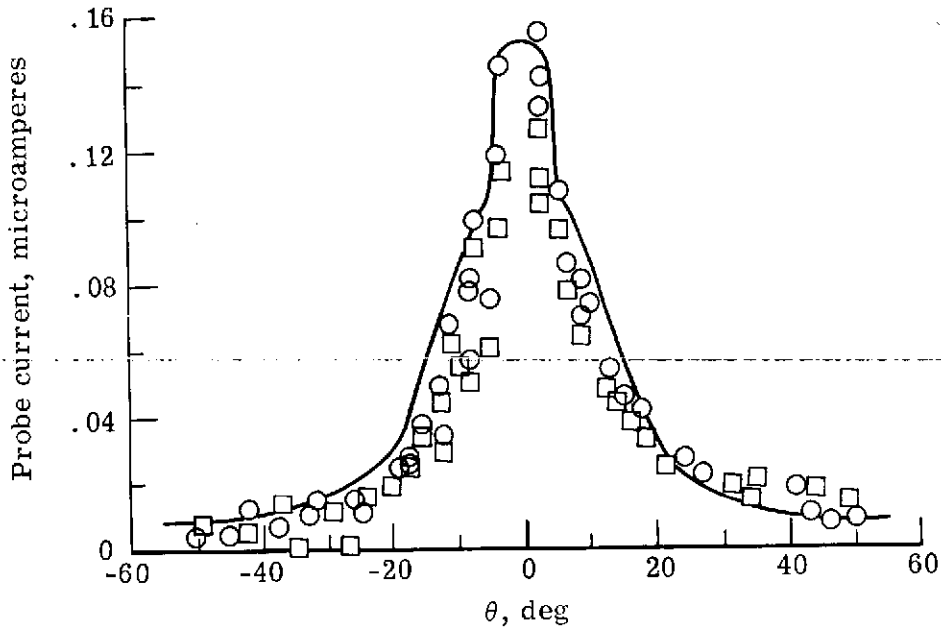

Figure 13.- The theoretical ion current computed by present theory for Bettinger and Chen's data. (The circular symbols correspond to the dots of fig. 1 and the squares correspond to the X's of the same figure.) Note that all the data of figure 1 have not been transferred; however, all the extreme points have been transferred.

Class II, subclass B.- Unfortunately, the data of Hester and Sonin (ref. 3) are presented (fig. 2) in nondimensional form, and the electron number density is not given. Thus, an exact analysis is precluded. However, sufficient data are presented to support an analysis of the curve shape to be expected. Reference 3 complements the data of figure 2 with the following data:

$$r_p = 0.127 \text{ mm}$$

$$\frac{T_i}{T_e} \leq 10^{-2}$$

$$T_i \text{ near zero}$$

24

Thus λ_D, L, and T_e are found to be, respectively, 1.651 mm, 57.15 mm, and $\geqq T_i/10^{-2}$. At this point it is necessary to assume a value for T_i and to assume $T_e = T_i/10^{-2}$.

Assume that $T_i = 2$ K (near zero) yields a T_e of 200 K. Since values for the electron temperature T_e and Debye length λ_D are known, the electron number density n can be calculated from the definition of λ_D. Such a computation results in an n of 3.19×10^{11} electrons/m^3. The ratio E of bulk flow velocity U to the ion velocity V_+ is given as 38, and V_+ is computed[1] as 204 m/sec and results in a U of 7753 m/sec. By proceeding as in the example for subclass A, t_+, d_+, ψ_{min}, θ_1, θ_2, and θ_3 are calculated as 6.793×10^{-7} sec, 5.266 mm, 4.09^O, 7.07^O, 18.58^O, and 19.67^O, respectively.

Theoretical values of ion current can now be computed[2] by equation (9), and non-dimensionalized by using the current at zero angle of attack as a normalizing factor. The nondimensional ion current thus obtained is presented in figure 14. A comparison of the shape of this theoretical curve with the shape of the data curve of figure 2 gives good general agreement. An exact agreement was not expected since exact values of T_i and T_i/T_e were not known.
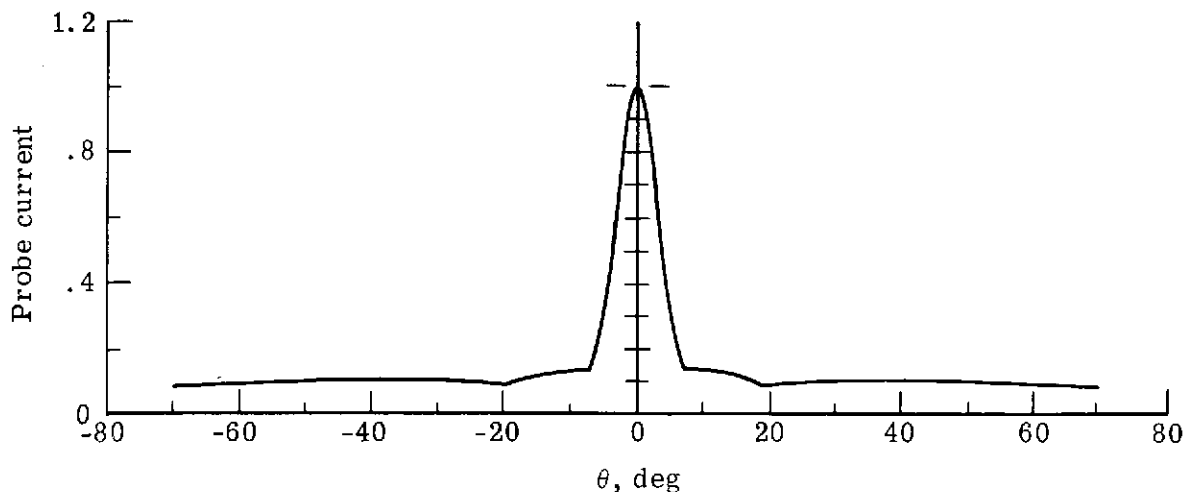

Figure 14.- The theoretical nondimensional ion current for the data of reference 3. $T_i = 2$ K and $T_e = T_i/10^{-2}$. (Peak current has a dimensional value of 0.0656 microampere.)

To eliminate the possibility that the agreement for these curves is due to a fortuitous choice of T_i (2 K), two other curves using different values of T_i were computed.

[1]The ions were singularly ionized argon (A^+).

[2]The $\sin \psi_m$ should have several decimal places to prevent errors in $\left(\sin \psi_m\right)^A$ since A can be large; that is, here A = 38, 1, or 0.

Assumed ion temperatures T_i of 15 K and 150 K result in electron number densities of 2.69×10^{12} and 2.69×10^{13} electrons/m^3. With $T_e = T_i/10^{-2}$, the electron temperatures are 1500 K and 15 000 K, respectively. The corresponding nondimensional ion current curves are presented in figures 15 and 16. The shapes of these curves are also in good general agreement with the data curve of figure 2.
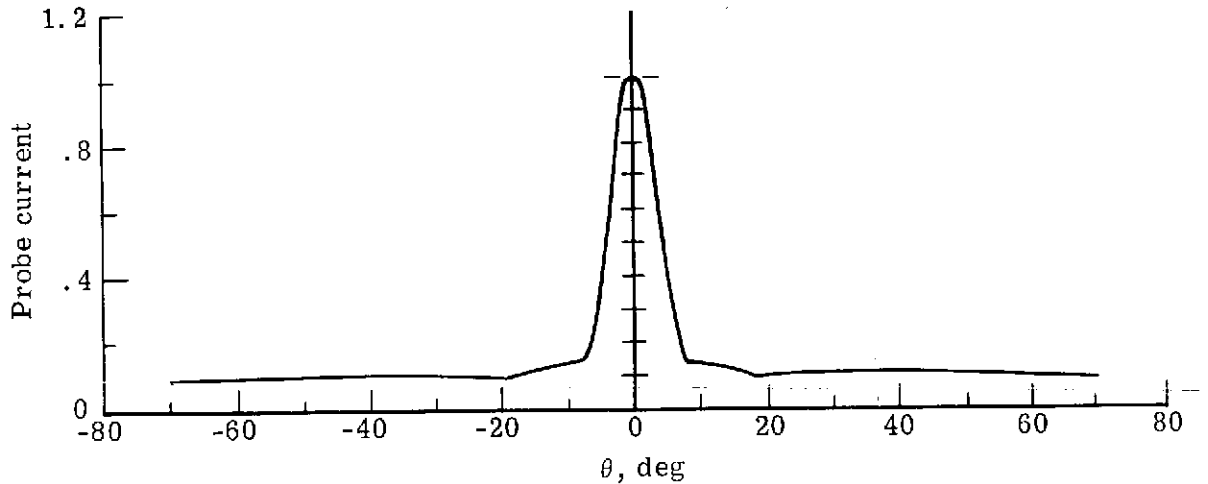

Figure 15.- The theoretical nondimensional ion current for the data of reference 3. T_i = 15 K and $T_e = T_i/10^{-2}$. (Peak current has a dimensional value of 1.285 microamperes.)
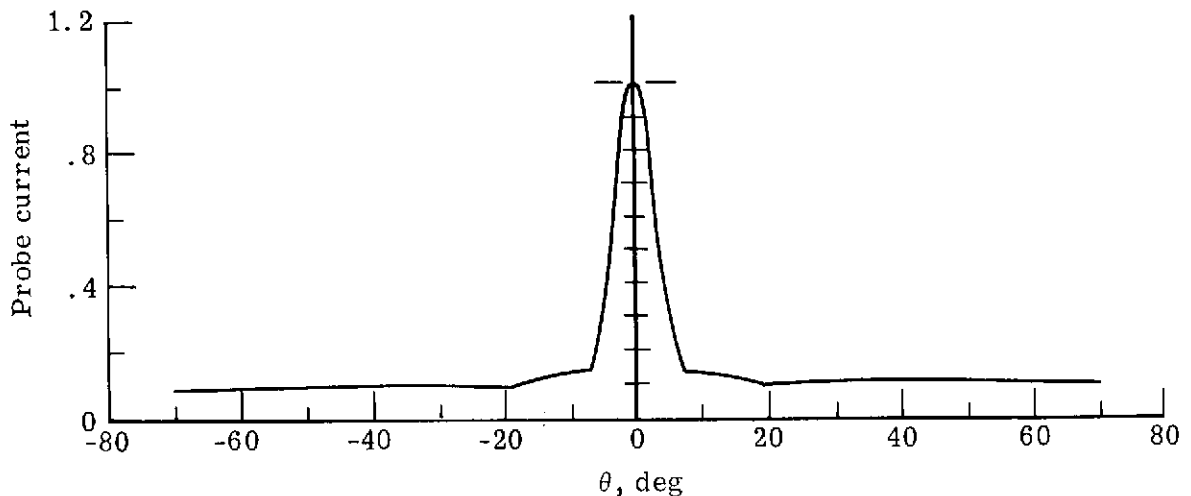

Figure 16.- The theoretical nondimensional ion current for the data of reference 3. T_i = 150 K and $T_e = T_i/10^{-2}$. (Peak current has a dimensional value of 38.534 microamperes.)

Electron Temperature Determination Using Present Theory

__Thermal (class I).-__ At zero angle of attack $\theta = 0^O$, equation (7) becomes

$$I = 2en\pi(\lambda_D + r_p)(L - d_+)V_+ - 2en\pi(\lambda_D + r_p)(L - d_{-r})(V_-)\exp\left(-\frac{e\phi_p}{KT_e}\right)$$
$$+ enU(r_p + \lambda_D)^2\pi - enU(r_p)^2\pi$$

For the electron-retarding region of the response curve (fig. 3), this equation can be written as

$$I = 2en\pi(\lambda_D + r_p)(L)V_+ - 2en\pi(\lambda_D + r_p)(L)(V_-)\exp\left(-\frac{e\phi_p}{KT_e}\right)$$
$$+ 2nU\pi(r_p + \lambda_D)^2 - en\pi U(r_p)^2$$

since neither d_+ nor d_{-r} is an appreciable part of L. If

$$I_+ = 2en\pi(\lambda_D + r_p)(L)(V_+)$$

$$I_- = -2en\pi(\lambda_D + r_p)(L)(V_-)$$

and

$$I_{end} = enU\pi(r_p + \lambda_D)^2 - enU(r_p)^2\pi$$

then

$$I = I_+ + I_{end} + (I_-)\exp\left(-\frac{e\phi_p}{KT_e}\right)$$

By taking the natural logarithm and differentiating with respect to ϕ_p, one gets $\frac{d}{d\phi_p}\left[\log_e(I - I_+ - I_{end})\right] = \frac{-e}{KT_e}$. But since $\phi = V - V_p$ and V_p is constant $d\phi_p = dV$.

Thus $\frac{d\log_e(I - I_+ - I_{end})}{dV} = \frac{-e}{KT_e}$ and T_e can be found by plotting the current against voltage. On semilog paper, such a plot is a straight line with slope $\frac{e}{KT_e}$. The electron temperature is easily computed once the slope is obtained, e and K being known physical constants.

This plotting procedure is exactly the same as that used by Langmuir, Laframboise, Sonin, etc. to find the electron temperature. Even though it was demonstrated only for parallel probe alinement, it is a simple matter to show that it holds for arbitrary orientation angle. Experimentally, the present authors determined the same electron

temperatures for various angles of attack. Sonin also obtained the same electron temperatures for various angles of attack (ref. 6).

Flow-Directed (Class II) Theory

The theory for subclasses A and B of Class II is valid only in the ion-saturation region of the response curve (fig. 3) where only ions are collected. As a consequence of no electron collection, the electron temperature cannot be determined by using the theory of Class II. Fortunately, in the electron-retarding region of the response curve, electrons are again collected. This electron collection produces an electron current hundreds of times greater than the ion current and means that nearly all the total current is due to thermal motion. The criterion for Class I is thus satisfied. This result illustrates how classes can be switched (Class II to Class I only) by varying the voltage, so that results in the electron-retarding region of the response curve can be obtained. Therefore, the electron temperature T_e can be obtained by the procedure presented for class I.

Class Determination

The application of the theory for one class to data of another class results in gross errors; therefore, the data should be correctly classed with the theory.

Although final classification must be determined by applying the class criteria at an angle of attack of 0°, there are certain other characteristics which are helpful. Class I (thermal) current data for flowing plasma plotted against orientation angle θ, for example, has a valley point at an angle of attack of 0°. A similar plot of Class II (subclasses A and B) current data has a peak point at θ equal zero. The distinctiveness of the valleying and peaking effects is directly related to the bulk flow velocity U and the ion velocity V_+. Class I data for a slow flowing plasma with high V_+ would have an indistinct valley. In fact, a flow velocity U of zero would result in a straight line, since the current is independent of the orientation angle for a stationary plasma. Higher flow velocities produce more pronounced valleys. The peaking of Class II is dominated by the ratio E of the bulk flow velocity to the ion velocity. As the ratio E increases, the peaking becomes sharper.

Recall also that the ratio E is used to determine whether subclass A or B is represented. Knowing that certain data are of the Class II type is meaningless by itself. The bulk flow velocity U and the ion velocity V_+ must be known (or V_+ is computed from knowledge of values of T_e and m_i). With U and V_+ known, E is computed. If E is less than 10, then the data belong to subclass A, and if E is greater than 10, they belong to subclass B.

APPLICATIONS

It is readily apparent, from the valleying and peaking characteristics of the curves of ion current against angle of attack of this work, that electrostatic probes can be used to determine local plasma flow direction. This is done by simply recording the orientation of the probe as it is pivoted and rotated until the valley or peak point current is reached. With this orientation the probe axis is parallel to the local flow; hence, the flow direction is that of the probe axis.

There is also the possibility of using the theory to determine the ion density and flow velocity.

By using a general curve-fit procedure or a theoretically computed family of curves (curves of current against n with E, F, λ_D, etc. determining the members of the family), it should be possible to obtain the ion density. A curve-fit scheme would probably be more accurate; undoubtedly, it would be complex and tedious and would involve one or more iterative procedures.

Since the ion current for various angles of attack is highly dependent on the flow velocity, one may be able to extract the velocity through some analytical manipulation of the ion currents for two or more angles of attack. If n is known, then the coefficients E and F can be determined empirically. The definition of E (or F) could then be used to obtain the velocity. This second approach, unfortunately, requires an independent measure of the ion density.

CONCLUSIONS

In the experimental part of this work, a microwave interferometer and an electrostatic probe array have been used to measure the electron number density in the free stream of a 1-foot arc-heated hypersonic wind tunnel (30.5 cm). The electrostatic probe technique also yielded electron temperature measurements. Both types of measurements were made for a wide range of tunnel free-stream conditions with air and nitrogen as test media.

The analytical part of this work consisted of the development of a general theory for calculating the ion current collected by a cylindrical electrostatic probe oriented at arbitrary angles of attack in a flowing plasma. This theory is composed of two central classes (Class I (thermal) and Class II (flow-directed)). Class II is further divided into subclasses A and B. It was not determined whether there are conditions for which both Class I and Class II theory are equally valid. Nor were the conditions for switching from Class I to Class II obtained.

The significant conclusions are as follows:

1. The present theory is applicable to a wide range of flowing plasma conditions.

2. By using the present theory, the electron temperature is determined by the semilog method previously developed.

3. The peaking and "valleying" of ion current is not the result of end effect per se, but the consequence of side collection which is highly dependent on angle of attack, and the ratio of the flow velocity to the ion velocity.

4. The theory of this report is in good agreement with Sonin's algorithm results, when applied to the conditions of the test series (parallel alinement only). (No end effect was detected.)

Langley Research Center,
    National Aeronautics and Space Administration,
        Hampton, Va., March 26, 1974.

APPENDIX A

THE NONCOLLECTION LENGTHS d_+ AND d_{-r}

If a cylindrical probe (see fig. 17), having a potential V, is immersed in plasma of effective potential V_p, it will collect charged particles (ions or electrons). The particles collected are limited to those within a region extending a Debye length λ_D from the surface of the probe at any one time. (The Debye length is the maximum distance at which a charged body can affect other charged bodies in a plasma.) Since the surface of the probe is cylindrical in shape, the imaginary surface (Debye shield) that encloses this region is a cylindrical shell capped by a hemispherical shell. A plasma flowing parallel ($\theta = 0°$) to the axis of the probes interprets the Debye shield as a cylindrical shell capped by a disk, since it projects the hemisphere as a circular disk. Therefore, this shape is assumed for the Debye shield (fig. 17) for all small angles of orientation.
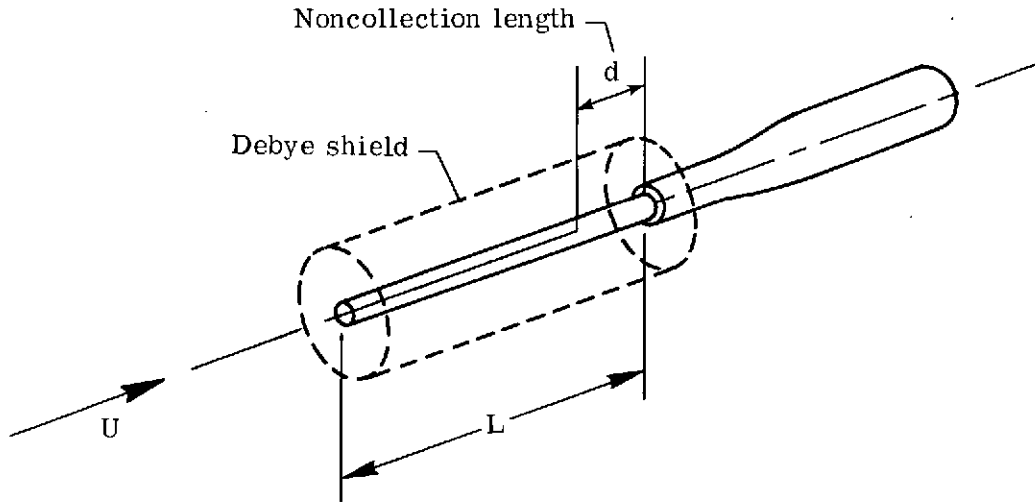
Figure 17.- Probe with its cylindrical Debye shield.

The particles outside the Debye shield are not influenced by the probe's presence (where it is assumed that the probe creates no shock waves). Upon entering the shield they are affected by the probe because its electric field $\overline{E}$ influences them immediately.

This electric field $\overline{E}$ arises as a consequence of the potential difference $\left(\phi_p = V - V_p\right)$ between the shield and the probe. Furthermore, it can be concluded that the $\overline{E}$ field only varies radially with respect to the probe. This conclusion is readily deduced from the fact that the only possible $\overline{E}$ field is the one normal to both the equipotential surfaces of the probe and of the shield. The lines of the $\overline{E}$ field lie along the radii joining the probe and the shield, and its strength is

$$E_r = \frac{-\phi_p}{\lambda_D} \tag{A1}$$

The force acting radially on a charged particle that enters the $\overline{E}$ field is

$$F_r = qE_r = \frac{q\phi_p}{\lambda_D} \tag{A2}$$

The acceleration a_r that the particles of mass m_p experience in the $\overline{E}$ field can be written, by means of Newton's second law, as

$$a_r = \frac{dV}{dt} = \frac{F_r}{m_p} \tag{A3}$$

which can be rewritten by using equation (A2) as

$$\frac{dV}{dt} = \frac{q\phi_p}{m_p\lambda_D} \tag{A4}$$

Separating variables and integrating gives velocity as a function of time

$$V(t) = \frac{q\phi_p t}{m_p\lambda_D} + C_i \tag{A5}$$

where C_i is the constant of integration. By applying the boundary condition at time zero, the particle enters the shield with initial velocity V_o and gives the value of the constant C_i as V_o. Equation (A5) can be written as

$$V(t) = \frac{q\phi_p t}{m_p\lambda_D} + V_o \tag{A6}$$

The velocity $V(t)$ can also be written as the time rate of change of the coordinate going from the shield to the probe $V(t) = \frac{dr}{dt}$. Making this substitution into equation (A6) gives

$$\frac{dr}{dt} = \frac{q\phi_p t}{m_p\lambda_D} + V_o \tag{A7}$$

By integrating and applying the boundary condition $r = 0$ at $t = 0$ (the instant that particles enter the field), it is found that

$$r = \frac{q\phi_p t^2}{2m_p\lambda_D} + V_o t \tag{A8}$$

This equation can be used to calculate the total time t that it takes for the particles to travel from the shield to the probe if the distance r is replaced with λ_D. If the potential difference ϕ_p is negative, then ions are accelerated toward the probe and equation (A8) for an ion is

$$\frac{q\phi_p t_+^2}{2m_i\lambda_D} + V_+ t_+ - \lambda_D = 0 \tag{A9}$$

For an electron, equation (A8) becomes

$$\frac{-q\phi_p\left(t_{-r}\right)^2}{2m_e\lambda_D} + V_- t_{-r} - \lambda_D = 0 \tag{A10}$$

By solving equation (A9) for the time $\left(t_+\right)$ that it takes ions to travel from the Debye shield to the probe surface, the roots are

$$t_+ = \frac{-\left(V_+\right)m_i\lambda_D}{q\phi_p} \pm \frac{\lambda_D m_i\sqrt{V_+^2 + \left(2q\phi_p/m_i\right)}}{q\phi_p}$$

The root that is desired is

$$t_+ = \frac{-m_i\lambda_D V_+}{q\phi_p} + \frac{\lambda_D m_i\sqrt{V_+^2 + 2q\phi_p/m_i}}{q\phi_p} \tag{A11}$$

The other root is useless since it is negative and negative time has no relevance here. Multiplying equation (A11) by the bulk flow velocity U gives the length d_+ for which no ions are collected. This length is

$$d_+ = Ut_+ = \frac{-V_+\lambda_D m_i U}{q\phi_p} + \frac{\lambda_D m_i U\sqrt{V_+^2 + 2q\phi_p/m_i}}{q\phi_p} \tag{A12}$$

By solving equation (A10) for the time t_{-r} it takes a decelerating electron to reach the probe, the following roots are obtained:

$$t_{-r} = \frac{m_e\lambda_D V_-}{q\phi_p} \pm \frac{\sqrt{m_e}\,\lambda_D\sqrt{2}}{q\phi_p}\sqrt{\frac{m_e V_-^2}{2} - q\phi_p} \tag{A13}$$

It is immediately apparent that both roots are imaginary if the kinetic energy $\dfrac{m_e V_-^2}{2}$ of the electron as it enters the shield is less than the potential energy $q\phi_p$ of

the field. Physically, this condition means that no such electron can reach the probe. If all electrons entering the shield have kinetic energies less than the potential energy of the field, the noncollection length d_{-r} is exactly equal to the probe length L. (This condition requires the second term of eq. (10) to vanish.) Equation (A13) represents two real roots when the electron has kinetic energy sufficient to overcome the field and reach the probe. However, only the root

$$t_{-r} = \frac{m_e \lambda_D V_-}{q \phi_p} - \frac{\sqrt{2m_e} \lambda_D}{d \phi_p} \sqrt{\frac{m_e V_-^2}{2} - q \phi_p} \tag{A14}$$

is physically possible. The other root would require the time t_{-r} to increase as the entry velocity of the electron increases. This increase is impossible since less time is needed to travel a certain distance as the velocity of travel is increased.

The noncollection length d_{-r} for electrons in a plasma of bulk velocity U is

$$d_{-r} = U t_{-r} = \frac{U m_e \lambda_D V_-}{q \phi_p} - \frac{\sqrt{2m_e} \lambda_D U}{q \phi_p} \sqrt{\frac{m_e V_-^2}{2} - q \phi_p} \tag{A15}$$

In the special case where $\phi_p = 0$, equations (A9) and (A10) reduce, respectively, to

$$V_+ t_+ - \lambda_D = 0$$

$$V_- t_{-r} - \lambda_D = 0$$

Solving these equations gives $t_+ = \lambda_D/V_+$ and $t_{-r} = \lambda_D/V_-$. Therefore, when $\phi_p = 0$, the ion and electron noncollection lengths are, respectively,

$$d_+ = U t_+ = \frac{U \lambda_D}{V_+}$$

$$d_{-r} = U t_{-r} = \frac{U \lambda_D}{V_-}$$

APPENDIX B

THE MAXIMUM ANGLE OF COLLECTION ψ_m

A probe oriented so that its axis forms an angle θ with a plasma flowing with velocity U has a component of velocity $U \sin \theta$ across it. As a result of the velocity component across the probe, not all the ions that enter the Debye shield are collected. This result is a consequence of the trajectories that ions in the field must have. Any ion entering the shield at a point such as point A of figure 18 would follow a slightly curved trajectory. This curved trajectory takes the ion out of the shield where it cannot be collected; whereas, if the point of entry is shifted along the shield, from A toward C, a point B will be reached where the entry will result in collection. Ions entering between B and C all have trajectories which carry them to the probe surface where they are collected.
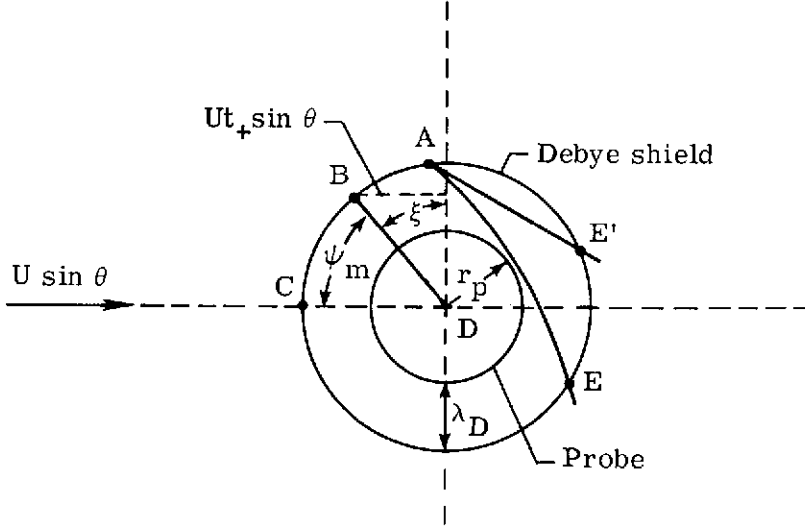

Figure 18.- Cross section of probe and its Debye shield taken perpendicular to the probe axis. AE and AE' are exaggerated trajectories of noncollection.

The angle ψ_m formed by the lines joining B and D and C and D is the maximum angle of collection. Calculating this angle by using the trajectories of ions is difficult, if not impossible. Fortunately, the noncollection angle ξ can be calculated easily and thus ψ_m can be found. By referring to the geometry of figure 18, the side of the triangle opposite the angle ξ has a minimum value of $U t_+ \sin \theta$. The hypotenuse $\overline{BD}$ of this triangle is $\lambda_D + r_p$. This angle of noncollection in degrees is

$$\xi = \text{arc } \sin\left(\frac{U t_+ \sin \theta}{\lambda_D + r_p}\right) \tag{B1}$$

Since ψ_m and ξ must sum to form a right angle, the angle of maximum collection is

$$\psi_m = 90^O - \xi = 90^O - \text{arc } \sin\left(\frac{Ut_+ \sin \theta}{\lambda_D + r_p}\right) \tag{B2}$$

Note that the angle θ has one unique ψ_m associated with it and that ψ_m decreases as θ increases. This trend is valid until the angle $\theta = \theta_3$ for which ψ_m equals ψ_{min} is reached. For all θ values above θ_3, the maximum angle of collection has its minimum value of ψ_{min}.

By referring to figure 19, the angle ψ_m can be no smaller than one half the angle subtended by the chord created by projecting the diameter of the probe onto the shield.
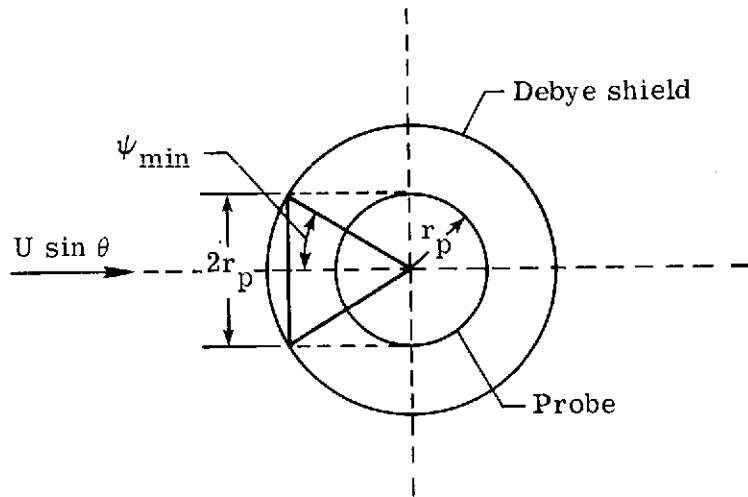

Figure 19.- Cross section of probe and shield showing geometry used in determining a minimum value of ψ_m.

Therefore,

$$\psi_{min} = \text{arc } \sin\left(\frac{r_p}{\lambda_D + r_p}\right) \tag{B3}$$

is the minimum value of ψ_m. Now with ψ_{min} and equation (B2) the orientation angles θ_1 and θ_2, with transitions 1 and 2, can be calculated. Transition 1 takes place at

$$\sin \psi_m = \exp\left(\frac{\log_e \sin \psi_m}{E - 1}\right) \tag{B4}$$

By means of equation (B3) this equation can be rewritten as

$$\sin \psi_m = \exp\left\{\frac{\log_e\left[r_p/(\lambda_D + r_p)\right]}{E - 1}\right\} \tag{B5}$$

Therefore,

$$\psi_m = \text{arc } \sin\left(\exp\left\{\frac{\log_e\left[r_p/(\lambda_D + r_p)\right]}{E - 1}\right\}\right) \tag{B6}$$

Substituting this value of ψ_m into equation (B2) gives

$$\text{arc } \sin\left(\exp\left\{\frac{\log_e\left[r_p/(\lambda_D + r_p)\right]}{E - 1}\right\}\right) = 90^o - \text{arc } \sin\left(\frac{Ut_+ \sin \theta_1}{\lambda_D + r_p}\right) \tag{B7}$$

Equation (B7) is easily solved for the first transition-point orientation angle θ_1. Since transition 2 occurs when $\sin \psi_m = \sin \theta_2$, then ψ_m must equal θ_2 and ψ_m can be replaced with θ_2 in equation (B2). If 90° is subtracted from both sides of equation (B2) after this replacement, then equation (B2) becomes

$$\theta_2 - 90^o = -\text{arc } \sin\left(\frac{Ut_+ \sin \theta_2}{\lambda_D + r_p}\right) \tag{B8}$$

Taking the sine of equation (B8) gives

$$\sin\left(\theta_2 - 90^o\right) = \frac{-Ut_+ \sin \theta_2}{\lambda_D + r_p} \tag{B9}$$

By using the trigonometric identity, $\sin(a - b) = \sin a \cos b - \sin b \cos a$, equation (B9) can be reduced to

$$-\cos \theta_2 = \frac{-Ut_+ \sin \theta_2}{\lambda_D + r_p} \tag{B10}$$

If equation (B10) is divided by $\sin \theta_2$ and multiplied by -1, it becomes

$$\frac{\cos \theta_2}{\sin \theta_2} = \cot \theta_2 = \frac{Ut_+}{\lambda_D + r_p} \tag{B11}$$

Inversion gives

$$\tan \theta_2 = \frac{\lambda_D + r_p}{Ut_+} \tag{B12}$$

Thus the second transition-point orientation angle θ_2 is

$$\theta_2 = \arctan\left(\frac{\lambda_D + r_p}{Ut_+}\right) \tag{B13}$$

The orientation angle θ_3 where the maximum angle of collection reaches its minimum value can be found by replacing ψ_m in equation (B2) by its minimum value of equation (B3).

REFERENCES

1. Bettinger, Richard T.; and Chen, A. Anthony: An End Effect Associated With Cylindrical Langmuir Probes Moving at Satellite Velocities. J. Geophys. Res., vol. 73, no. 7, Apr. 1, 1968, pp. 2513-2528.

2. Hester, S. D.; and Sonin, A. A.: Some Results From a Laboratory Study of Satellite Wake Structure and Probe Response in Collisionless Plasma Flows. Rarefied Gas Dynamics, Vol. II, Leon Trilling and Harold Y. Wachman, eds., Academic Press, Inc., 1969, pp. 1659-1670.

3. Hester, S. D.; and Sonin, Ain A.: An Ion Temperature Sensitive End Effect in Cylindrical Langmuir Probe Response at Ionospheric Satellite Conditions. Publ. No. 69-9 (Contract Nonr-1841(93)), Fluid Mech. Lab., Massachusetts Inst. Technol., Sept. 1969. (Also Phys. Fluids, vol. 13, no. 5, May 1970, pp. 1265-1274.)

4. Laframboise, James G.: Theory of Spherical and Cylindrical Langmuir Probes in a Collisionless, Maxwellian Plasma at Rest. Rep. No. 100, Inst. Aerosp. Studies, Univ. of Toronto, June 1966. (Available from DDC as AD 634596.)

5. Sonin, A. A.: The Behavior of Free Molecule Cylindrical Langmuir Probes in Supersonic Flows, and Their Application to the Study of the Blunt Body Stagnation Layer. UTIAS Rep. No. 109, Univ. of Toronto, Aug. 1965.

6. Sonin, Ain A.: Free-Molecule Langmuir Probe and Its Use in Flowfield Studies. AIAA J., vol. 4, no. 9, Sept. 1966, pp. 1588-1596.

7. Dunn, Michael G.; and Lordi, John A.: Thin-Wire Langmuir-Probe Measurements in the Transition and Free-Molecular Flow Regimes. AIAA J., vol. 8, no. 6, June 1970, pp. 1077-1081.

8. Duckett, Roy J.; and Jones, W. Linwood, Jr.: Free-Stream Electron Concentration in an Arc-Heated Wind Tunnel and Correlation of Langmuir Probe and Microwave Interferometer Measurements. NASA TN D-5500, 1969.

9. Loeb, Leonard B.: Basic Process of Gaseous Electronics. Univ. of California Press, 1955.

10. de Leeuw, J. H.: Electrostatic Plasma Probes. Physico-Chemical Diagnostics of Plasmas, Thomas P. Anderson, Robert W. Springer, and Richard C. Warden, eds., Northwestern Univ. Press, 1963, pp. 65-95.

11. Mott-Smith, H. M.; and Langmuir, Irving: The Theory of Collectors in Gaseous Discharges. Phys. Rev., vol. 28, Oct. 1926, pp. 727-763.

12. Bernstein, Ira B.; and Rabinowitz, Irving N.: Theory of Electrostatic Probes in a Low-Density Plasma. Phys. Fluids, vol. 2, no. 2, Mar.-Apr. 1959, pp. 112-121.

13. Heald, M. A.; and Warton, C. B.: Plasma Diagnostic With Microwaves. John Wiley & Sons, Inc., c.1965.

14. Cohn, Seymour B.; and Oltman, H. George: A Precision Microwave Phase-Measurement System With Sweep Presentation. 1961 IRE International Convention Record, vol. 9, pt. 3, Inst. Radio Eng., Mar. 1961, pp. 147-150.

15. Boatright, W. B.; Stewart, R. B.; and Sebacher, D. I.: Testing Experience and Calibration Experiments in a Mach Number 12, 1-Foot Hypersonic Arc Tunnel. Third Hypervelocity Techniques Symposium (Denver, Colo.), Mar. 1964, pp. 182-212.

16. Boatright, W. B.; Sebacher, D. I.; Guy, R. W.; and Duckett, R. J.: Review of Testing Techniques and Flow Calibration Results for Hypersonic Arc Tunnels. AIAA Paper No. 68-379, Apr. 1968.

17. Duckett, Roy J.; and Sebacher, Daniel I.: Velocity Measurements in the Langley 1-Foot (0.305-Meter) Hypersonic Arc Tunnel. NASA TN D-3308, 1966.

18. Guy, Robert W.: A Calibration and Diagnosis of the Test Stream of an Electric Arc-Heated Wind Tunnel. M.A.E. Thesis, Univ. of Virginia, Sept. 1969.